Chapter 8
Proton-fountain Electric-field-assisted Nanolithography (PEN)

Andres La Rosa and Mingdi Yan

Abstract This chapter describes the implementation of Proton-fountain Electric-field-assisted Nanolithography (PEN) as a potential tool for fabricating nanostructures by exploiting the properties of stimuli-responsive materials. The merits of PEN are demonstrated using poly(4-vinylpyridine) (P4VP) films, whose structural (swelling) response is triggered by the delivery of protons from an acidic fountain tip into the polymer substrate. Despite the probably many intervening factors affecting the fabrication process, PEN underscores the improved reliability in the pattern formation when using an external electric field (with voltage values of up to 5 V applied between the probe and the sample) as well as when controlling the environmental humidity conditions. PEN thus expands the applications of P4VP as a stimuli-responsive material into the nanoscale domain, which could have technological impact on the fabrication of memory and sensing devices as well as in the fabrication of nanostructures that closely mimic natural bio-environments. The reproducibility and reversible character of the PEN fabrication process offers opportunities to also use these films as test bed for studying fundamental (thermodynamic and kinetic) physical properties of responsive materials at the nanoscale level.

Keywords Responsive materials · P4VP · Nanolithography · Swelling · Polymer film · pH responsive · Erasable patterns · PEN · Biomimetic materials · DPN · Hydrogels · Osmotic pressure · Entropy of mixing · Protonation

8.1 Introduction

8.1.1 PEN as a Method for Creating Erasable Nanostructures

The applications of tip-based nanolithography techniques that create patterns by anchoring molecules *onto* a surface of proper chemical affinity – as is the case in dip-pen nanolithography (DPN) [1, 2] – can be expanded by, alternatively, triggering the formation of nanostructures out of stimuli-responsive material

A. La Rosa (✉)
Department of Physics, Portland State University, Portland, OR 97201, USA
e-mail: andres@pdx.edu

A.A. Tseng (ed.), *Tip-Based Nanofabrication*, DOI 10.1007/978-1-4419-9899-6_8,

substrates. Since stimuli-responsive properties may have a reversible character, the alternative nanofabrication approach could have concomitant implications in bio-technology (for creating switching gates that allow manipulating the transport, separation, and detection of bio-molecules, or for fabricating soft-material nanostructures that closely mimic natural bio-environments) as well as in emerging nano-electronics technologies (for fabricating low-cost and low-voltage operation integrated logic circuits in flexible substrates). The potential technological implications that can be brought by harnessing the fabrication of nanostructures out of stimuli responsive materials underlines the interest for developing Proton-fountain Electric-field-assisted Nanolithography (PEN). In PEN the formation of nanostructures is triggered by the localized injection of protons into the substrate, with the charge-transfer from a sharp tip into the substrate being better controlled by the application of an external electric field. The development of PEN is thus conceived within the context of emerging developments in materials science and molecular engineering [3] that pursue the design of devices that rely on the transduction of environmental signals.

8.1.2 PEN in the Context of Emerging Biomimetic Engineering

Inspired by the multi-functional inner working properties of living cell membranes [4], including the surprising sensitivity of their dynamic response to the mechanical properties of surrounding material [5], a current focus in biomimetic materials constitutes the development of versatile synthetic thin films that can selectively respond to a variety of signal interactions (mechanical, chemical, optical, changes in environmental conditions, etc) [6]. In one approach, the complex synthetic hierarchy needed to eventually mimic *nature* is conceived as a combination of functional-domains separated by stimuli-responsive polymer thin films regulating the interactions between the domain compartments [7]. In another approach, the cell is conceived not just as a chemical but also as a mechanical device [8], for it is found that the cell membrane is very sensitive to the mechanical properties of its surrounding matrix (affecting their growth, differentiation, migration, and, eventually, apoptosis) [9, 10], which has triggered an interest in the development of, for example, synthetic polymer scaffold for regenerative medicine [11, 12]. Both approaches, mentioned above, emphasize the need for harnessing the fabrication of synthetic thin film responsive materials.

The different approaches to biomimetic materials have resulted in the design of a variety of responsive building blocks (gels [13], brushes [14], hybrid systems with inorganic particles [15]) that respond selectively to different (pH [16], temperature [17, 18], optical [15, 19], and magnetic [20]) external stimuli. Following the "bottom-up" route, functional materials have been prepared based on self-assembly of polymeric supramolecules [21]. Progress following the alternative "top-down" approach includes the fabrication of stimulus responsive polymer brushes [22], growth of polymers from previously DPN-patterned templates [23], and chain

polymerization of monomolecular layer by local stimulation using a STM tip [24, 25] (followed up by investigation of their working principle [26]). PEN falls in the top-down category approach. In the next section, we concentrate our description on hydrogels [27], since the latter describes closer the experimental results obtained in current applications of PEN.

8.2 Underlying Working Mechanisms of Swelling in Hydrogels

This section provides a succinct summary of the main theoretical results underlying the working mechanisms involved in the swelling of hydrogels, where the concept of entropy plays a key role. In particular, it is worth to highlight the peculiar theoretical framework brilliantly introduced, time ago, by Paul J. Flory [28, 29] for analyzing polymer solutions; although his models have been refined, the essence of his clever approach is still used. Given the expected complexity of these polymer structures, it results interesting to realize the conceptual similarities between (a) the analysis of a much simpler liquid-vapor system in equilibrium [30, 31], and (b) the analysis of the more complex (hydrogel) polymer solution [32] (see Fig. 8.1 below). For comparison and illustrative purposes both analyses will be presented here.

A hydrogel refers to a flexible (typically) hydrophilic cross-linked polymer network and a fluid filling the interstitial spaces of the network. The entire network holds the liquid in place thus giving the system a solid aspect. But contrary to other solid materials, these wet and soft systems are capable of undergoing very large

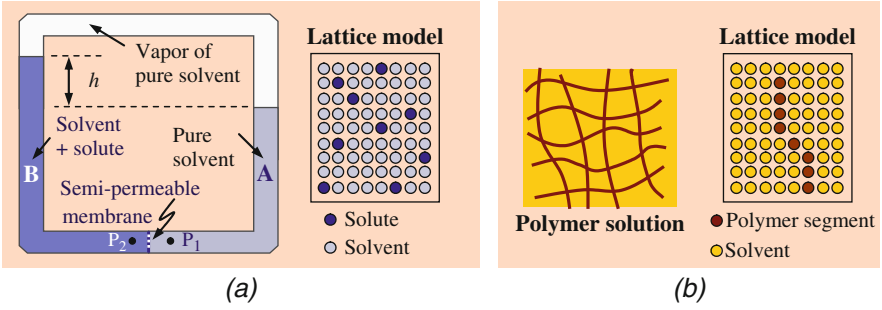

Fig. 8.1 Two different thermodynamic systems studied using similar lattice model analysis. (**a**) *Left:* Because of their different vapor pressures, a solution (water solvent + sugar solute molecules) and a pure water solvent (separated by a membrane permeable only to solvent molecules) generate an osmotic pressure ρgh (ρ is the density of the solution). *Right:* Solvent and solute molecules considered to reside in a hypothetical lattice, for entropy calculation purposes. The diagram on the *left* has been reproduced from Huang [30, p. 47] and reprinted with permission of John Wiley & Sons, Inc. (**b**) *Left:* Polymer gel system. *Right:* Polymer chain considered as solute immersed in solvent, where all molecules are considered to reside in a hypothetical liquid lattice. Figures adapted from Flory [32], Copyright @ 1953 Cornell University and Copyright @ 1981 Paul J. Flory; used by permission of the publisher, Cornell University Press

deformation (greater than 100%). Understanding the dynamic behavior of hydrogels is worthwhile to pursue due to their widespread implications. In particular, the role of gels in living organism can not be exaggerated. As it is well put by Osada and Gong [33], living organisms are largely made of gels (mammalian tissues are aqueous materials largely composed of protein and polysaccharide networks), which enables them to transport ions and molecules very effectively while keeping its solidity.

What drives the swelling in a hydrogel? One of the potential mechanisms can be described in terms of the osmotic pressure (an entropic driven phenomenon), which help us understand how the additional entropy of mixing (afforded by an increase in the system's volume due to the absorption of water by the polymer network) is counteracted by a restoring force (also of entropic origin, since a lager dimension afford less polymer configurations) from the network itself. This osmotic pressure refers to the same type of phenomenon underlying the lower vapor-pressure displayed by an ideal solution (solvent + non-volatile solute) when compared to the vapor-pressure of a pure solvent. Since the latter constitutes a much simpler and familiar process, we conveniently include its (brief) description in the next paragraph. More specifically, we address the dynamics involved when a solution (water solvent + sugar solute) and pure water solvent are separated by a semi-permeable membrane, which can help us gain knowledge about the osmotic pressure concept. The entropy of mixing involved in this phenomenon is described in the framework of a lattice model (one in which solute and solvent molecules are considered to reside on the sites of a hypothetical lattice, the latter used as a resource that facilitates the calculation of the solution's entropy). This approach will allow us to get familiar with lattice models, which are frequently used to describe polymer solutions (hydrogels). In short, we try to view the dynamics of hydrogels through the same prism used to view the equilibrium conditions of (water solvent + sugar solute) solutions.

8.2.1 The Osmotic Pressure in Ideal Liquid Solutions

The generation of a pressure difference (the osmotic pressure $\pi_{osmotic}$) across two phases as a consequence of their different vapor pressure is illustrated in Fig. 8.1a (see diagram on the left side). *Phase-A* (pure solvent water) and *phase-B* (solvent water + solute of sugar molecules) are separated by a membrane that allows the passage of water molecules but not the larger solute molecules [30]. It is an experimental fact that a dynamic equilibrium (i.e. equal rate, in both directions, of water molecules passing across the membrane) is reached when a hydrostatic pressure difference (the osmotic pressure $\pi_{osmotic}$) is established between the two phases. (Conceptually, the underlying mechanism at play here is that a water molecule in *phase-B* contributes greater to the total entropy than when inside the pure water *phase-A*; hence a net flow towards the former increases the total entropy.) The question to address is how to quantify this pressure difference.

8.2.1.1 Chemical Potentials of an Ideal Solution and a Pure Solvent

A formal description of the osmotic pressure [30, 31] takes into account the fact that under initial conditions of equal pressure P, the chemical potential $\mu^{A}_{\text{water},P}$ of water in *phase-A* (pure solvent water) is greater than the chemical potential $\mu^{B}_{\text{water},P}$ of water in *phase-B* (as it will be justified in the next paragraph and the next section below). Hence, when the phases are separated by a membrane permeable only to water, this constituent will not be in equilibrium and a net passage of water molecules from *phase-A* to *phase-B* is expected. As more water passes to *phase-B* the pressure increases and so does the chemical potential. Equilibrium with respect to the water constituent will then be established when $\mu^{B}_{\text{water},P_2}$ (the chemical potential of water in *phase-B*, at the increasing pressure P_2) becomes equal to $\mu^{A}_{\text{water},P_1}$ (the chemical potential of water in *phase-A*, at pressure P_1) [31]. The thus developed pressure difference $(P_2 - P_1)$ is referred to as the osmotic pressure, π_{osmotic}.

To find a relationship between the change in chemical potential and the osmotic pressure, let's resort first to the extensive properties of the thermodynamic potentials [34] (namely, when the amount of matter is changed by a given factor, they change by the same factor). A particular important relationship is obtained when this property is applied to the Gibbs free energy $G = G\,(T, P, N)$. In effect, being the temperature T and pressure P intensive quantities, G has to have the form

$$G = Nf(T, P),$$

where N is the number of particles of the analyzed system.

Since $\mathrm{d}G = -S\,\mathrm{d}T + V\,\mathrm{d}P + \mu\,\mathrm{d}N$ and $\mu = (dG/dN)_{T,P}$, the extensive property $G = Nf(T, P)$ implies that μ is only a function of T and P; that is,

$$\mu = G/N = f(T, P).$$

Accordingly, μ is the Gibbs free energy per molecule, and it is a quantity independent of N.

Thus,

$$d(G/N) = d\mu = -(S/N)dT + (V/N)dP,$$

which implies,

$$\frac{d\mu}{dP} = V/N.$$

This expression is pertinent to the quantification of the osmotic pressure. In effect, it reflects the change in chemical potential due to an increase in pressure, $\Delta\mu = (V/N)\,\Delta P$ (where it has been assumed that the volume does not change with pressure). Using $v \equiv (V/N)$, one obtains $\mu^{B}_{\text{water},P_2} - \mu^{A}_{\text{water},P_1} = v(P_2 - P_1)$, or,

$$\mu^{A}_{\text{water},P_1} - \mu^{B}_{\text{water},P_2} = v\pi_{osmotic} \tag{1}$$

8.2.1.2 Lattice Model for Calculating the Entropy of Mixing in Ideal Liquid Solutions

An explicit calculation of the chemical potential difference, in terms of the number of constitutive molecules, can be derived by starting (at the most fundamental level) from a relatively simple combinatorial analysis of dissimilar solvent (water) and solute (sugar) molecules allowed to reside on the sites of a hypothetical lattice (see the diagram at the right in Fig. 8.1a) [32], the latter introduced basically to facilitate the calculation the system's entropy of mixing ΔS_{mix}. In this lattice framework, the increase in the system entropy resulting from mixing N solvent and n solute molecules is given by $\Delta S_{\text{mix}}\ (N,n) = k\ \ln[(N + n)!/N!\ n!]$. For large values of N and n one can use the well known Stirling's approximation that gives $\ln n! = n \ln n - n \approx n \ln n$, or $n! \approx n^n$. Using this approximation, ΔS_{M} adopts the form $k \ln[(N + n)^{(N+n)}/N^N n^n]$, or

$$\Delta S_{\text{mix}}(N, n) = -k\ (N \ln f_N\ +\ n\ \ln f_n) \tag{2}$$

where $f_N \equiv N/(N + n)$ and $f_n \equiv n/(N + n)$ are the mole fractions of solvent (water) and solute (sugar) in the solution, respectively; k is the Boltzmann constant.

The Gibbs free energy has the general form $G = E + PV - TS = \mu N$. When applied to the system in *phase-B* (of N solvent and n solute molecules) at pressure P_2 and temperature T, one obtains,

$$G^{phase-B}(T, P_2, N, n) = G^{\text{pure}}_{\text{water}}(T, P_2, N) + G^{\text{pure}}_{\text{water}}(T, P_2, n) - T\Delta S_{\text{mix}}(N, n) \tag{3}$$

where the first two terms on the right hand side are the Gibbs energy of the corresponding components in their pure state (we are assuming an ideal solution, so the components do not interact).

The chemical potential of the water component in *phase-B* will then be given by,

$$\begin{aligned}
\mu^{phase-B}_{\text{water}}(T, P_2, N, n) &= \frac{dG^{phase-B}}{dN}(T, P_2, N, n) \\
&= \frac{dG^{\text{pure}}_{\text{water}}}{dN}(T, P_2, N) - T\frac{d}{dN}\Delta S_{\text{mix}} \\
&= \frac{dG^{\text{pure}}_{\text{water}}}{dN}(T, P_2, N) + kT\frac{d}{dN}(N \ln f_N + n \ln f_n) \\
\mu^{phase-B}_{\text{water}}(T, P_2, N, n) &= \mu^{\text{pure}}_{\text{water}}(T, P_2, N) + kT \ln f_N
\end{aligned} \tag{4}$$

For *phase-A*, which is constituted by pure water at pressure P_1,

$$\mu^{phase-A}_{\text{water}}(T, P_1, N, n = 0) = \mu^{\text{pure}}_{\text{water}}(T,\ P_1,\ N) \tag{5}$$

At equilibrium, $\mu_{\text{water}}^{phase-B}(T, P_2, N, n) = \mu_{\text{water}}^{phase-A}(T, P_1, N, n = 0)$. Therefore, expressions (4) and (5) lead to,

$$\mu_{\text{water}}^{\text{pure}}(T, P_2, N) - \mu_{\text{water}}^{\text{pure}}(T, P_1, N) = -kT \ln f_N \tag{6}$$

Replacing (6) in (1) gives,

$$\pi_{\text{osmotic}} = -\frac{kT}{\nu} \ln f_N = -\frac{kT}{V/N} \ln f_N \tag{7}$$

Incidentally, since we are working with solution where $f_n << 1$ and thus $\ln f_N = \ln(1 - f_n) = -f_n$, useful equivalent formulas can be obtained,

$$\pi_{\text{osmotic}} = \frac{kT}{V/N} f_n \text{ (for a dilute solution)} \tag{8}$$

or, by expanding further f_n, one gets $\pi_{\text{osmotic}} = \frac{kT}{V/N} \frac{n}{n+N} \approx kT \frac{n}{V}$.

$$\pi_{\text{osmotic}} \approx kT \frac{n}{V} = RT \frac{moles\ of\ solute}{V} = \frac{RT}{MW} \frac{mass\ of\ solute}{V} \tag{9}$$

where n is the number of solute molecules in a volume V, and MW is the solute's molecular weight.

8.2.2 *Lattice Model for Describing Ideal Polymer Solutions*

The basic results displayed by expressions (2) and (7) constitute a proper starting step for describing more complicated (and apparently unrelated) cases like, for example, a cross-linked polymer network interacting with a pool of water, i.e. a hydrogel. The elegant twist in the coming description lies in considering the polymer network as the solute[1] [32, 35]. That is, the trend of analysis using a hypothetical lattice conveniently remains the same; hence the observed similarity between the lattice displayed in Fig. 8.1a (used to analyze a liquid solution system) and the lattice in Fig. 8.1b (used to analyze a polymer solution) [36, 37]. In the latter, one polymer molecule is considered to be a chain of x segments, each segment (arbitrarily) considered equal in size to a solvent molecule. The objective becomes calculating the entropy of the polymer solution resulting from the different configurations that can be arranged with n_1 molecules of solvent and n_2 polymer molecules in a lattice containing $(n_1 + x\, n_2)$ cells.

[1] Lattice models of polymer solutions are widely used for their simplicity and computational convenience. Their use for predicting solution properties of polymers solutions dates back to the 1940s.

8.2.2.1 Lattice Model for Calculating the Entropy of Mixing

For the case of a polymer solution the calculation of the entropy can be conceived by counting first the different permutations associated with a given configuration of the polymer molecules (assuming no solvent molecules were present), and then adding the configurations resulting from their mixing with the solvent molecules (polymer segments and solvent molecules replacing one another in the liquid lattice). While the former is expected to contribute more effectively in a process of polymer fusion, here the interest focuses mainly on the entropy of mixing. The latter takes, quite surprisingly again, a very simple form [29, 32],

$$\Delta S_{\text{mixing}} = -k(n_1 \ln v_1 + n_2 \ln v_2) \tag{10}$$

where v_1 and v_2 are the volume fractions of solvent and solute respectively,

$$v_1 = n_1/(n_1 + xn_2)$$

$$v_2 = xn_2/(n_1 + xn_2)$$

Notice the similarity between expressions (2) and (10), except that volume fractions appear in the latter formula (mixing of molecules of different size) instead of mole fraction in the former (mixing of molecules of the same size).

8.2.2.2 The Heat Energy of Mixing ΔE_{M}, the Excluded Volume Effect, and the Helmholtz Free Energy ΔF_{M}

Given the fact that the dynamics of a polymer solution depends not only on the entropy but also on the energy of the system (the Helmholtz free energy $F = E - TS$ has to be minimum) this latter aspect is addressed in this section. In fact, the interactions between the water and the polymer molecules in a hydrogel make the polymer network a highly non-ideal thermodynamic system, where the cross-linked network structure plays an important role in determining the equilibrium aspects of the gel. In principle, any realistic model then has to take into account the intermolecular interactions due to the close proximity of the molecules, although some approximation can be applied depending on the temperature range being considered. On one hand, at relatively low temperatures a net attractive interaction between the monomers prevails, resulting in a net negative energy of the polymer system. On the other hand, at higher temperatures the repulsive interaction between the monomers when they are at very short distance (implicitly reflecting the fact that a monomer can not supplant the space already occupied by another monomer, a phenomenon better known in the jargon of polymer science as "excluded volume effect" or "excluded volume interaction") [38] will lead to a net positive energy of the polymer system. Below we provide some expressions that quantify this energy contribution.

In the lattice model, where each cell is able to accommodate either a solvent molecule or a polymer segment, the heat of mixing results from the replacement of some of the contacts between like-species (1-1 or 2-2) with unlike-constituents (1-2). If Δw_{12} represents the change in energy when one of these replacements occurs, then the heat associated with the formation of a particular configuration having p_{12} unlike-neighbors will be equal to $\Delta E_{\mathrm{M}} = p_{12}\ \Delta w_{12}$.

For the calculation of p_{12}, it is plausible to assume that the probability a particular site adjacent to a polymer segment is occupied by a solvent molecule to be proportional to the volume fraction v_1 of the solvent. On the other hand, if the number of cells which are first neighbor to a given cell is z (here z is expected to be on the order of 6–12), then zx is the number of contacts per polymer molecule, and zxn_2 would be proportional to the total number of contacts. p_{12} turns out to be then proportional to $(zxn_2)v_1$. On the other hand, using the definition $v_2 = xn_2/(n_1 + xn_2)$, one obtains $n_1 v_2 = xn_2\ n_1/(n_1 + xn_2) = xn_2\ v_1$. Hence, $\Delta E_{\mathrm{M}} = p_{12}\ \Delta w_{12} \sim (zxn_2)v_1 \Delta w_{12} = (z\ v_2\ n_1)\Delta w_{12} = (z\ \Delta w_{12})\ n_1\ v_2$. This result is typically expressed as,

$$\Delta E_{\mathrm{M}} = kT\ \chi_1\ n_1\ v_2 \tag{11}$$

where the quantity $kT\chi_1 \equiv z\ \Delta w_{12}$ characterizes (for a given solute) the interaction energy per solvent molecule.

As mentioned above, at relatively low temperatures the net contribution from this term has a negative value. However, at relatively high temperatures, it was pointed out early on by Flory that the interpretation of χ_1 should be expanded as to include also other potential interactions between neighboring components that could have concomitant (positive value) contribution to the Helmholtz free energy. The new interpretation relates χ_1 to the number of pair-molecules collisions [38], which should be proportional also to the number of pair contacts developed in the solution, just as for the heat exchange.

Using (10) and (11), the Helmholtz free energy of mixing is given by [32],

$$\begin{aligned} \Delta F_{\mathrm{mix}} &= \Delta E_{\mathrm{mix}} - \mathrm{T}\ \Delta S_{\mathrm{mix}} \\ &= kT(\ \chi_1\, n_1\, v_2 + n_1 \ln v_1 + n_2 \ln v_2\ ) \end{aligned} \tag{12}$$

8.2.3 Swelling of Neutral Polymer Networks

Notice that the above formulation basically describes the mixing of two liquids; the view of a polymer network held up by its cross-links has not appeared yet. The calculation given in (12), however, is a good initial step towards calculating the structural entropy of network formation. The latter was originally done in a very clever way by Paul Flory and John Rehner in their seminal papers [28, 29] (latter improved by Flory) [36], who modeled the cross-linked network as a system composed of v polymer chains of the same contour length (a chain counted as a

polymer thread between two cross-link intersections), with the location of the cross-link points positions defined, on average, on the vertex of a regular tetrahedron [28]. Any external distortion of the network (swelling, for example, due to the mixing of the polymers with a solvent) would be monitored by the distortion of this average tetrahedron cell.

In the Flory's description, the first step consists of calculating the different configuration that results from the dilution of v (short) polymer chains (prior to the cross-linking) with n solvent molecules. This is given by expression (10), with v playing the role of n_2,

$$\Delta S_{\mathrm{D}} = -k\left(n_1 \ln \frac{n_1}{n_1 + xv} + v \ln \frac{v_1}{n_1 + xv}\right) \tag{13}$$

This is followed by a more elaborated calculation of the additional entropy corresponding to the different configurations that lead to the formation of a network of tetrahedron cells in a sea of solvent molecules.

$$\Delta S_{V'} = \Delta S_{\mathrm{D}} + \Delta S_{\text{network of tetrahedron cells}} \tag{14}$$

Here the sub index V' stands for the final total volume of the swollen polymer network due to the mixing of the polymer with the solvent molecules. The objective here, however, is to calculate the net change in entropy $\Delta S_{\text{swelling}}$ due just to the swelling; that is,

$$\Delta S_{\text{swelling}} = \Delta S_{v'} - \Delta S_{v} \tag{15}$$

where ΔS_V stands for the entropy of the network when no solvent molecules are present. The result, in terms of the volume fraction $v_2 = x\, v/(n_1 + xv)$, is given by [36],

$$\Delta S_{\text{swelling}} = \underbrace{-kn_1 \ln(1 - v_2)}_{\text{Entropy of mixing polymers and solvent}} - \underbrace{\frac{3}{2} kv[(1/v_2)^{2/3} - 1]}_{\text{elastic entropy arising from the deformation of the network}} - \frac{1}{2} kv \ln v_2 \tag{16}$$

This expression reflects the contribution to the entropy from two different sources. Before dilution with the solvent molecules, the configuration of the network corresponds to one of maximum entropy, hence any deformation (due to swelling) would lead to a configuration of comparatively lower entropy. The latter then competes against the tendency for an entropy increase caused by the addition of solvent (and volume) that favors the creation of new configurations. Expression (15) embodies then the physical mechanism underlying the swelling process in an uncharged hydrogel. Using (11) and (15), the change in free energy is given by, $\Delta F = \Delta E_{\mathrm{M}} - T\,\Delta S_{\text{swelling}}$. Equilibrium is governed by the condition $\Delta F = 0$.

8.2.4 Swelling of Ionic Polymer Networks

Another potential channel for causing a polymer network to swell is the existence of charge centers, or molecular groups, which can strongly interact among themselves and with other ions contained in the solvent. That is the case in a poly(4-vinylpyridine) (P4VP), whose pyridyl groups can react with hydronium ions H_3O^+ thus forming positively charged nitrogen centers (N^+). The situation is depicted in Fig. 8.2. If the fixed pyridinium cations were the only ions present there would be an exceedingly large electrostatic repulsion, but such interaction is partially screened by the presence of counterions resulting from the dissociation of the phosphate salts in water,

$$\begin{aligned} &NaH_2PO_4 \rightarrow Na^+ + H_2PO_4^- \\ &H_2PO_4^- + H_2O \rightleftharpoons H_3O^+ + HPO_4^{2-} \quad K = 6.31 \times 10^{-8} \\ &HPO_4^{2-} + H_2O \rightleftharpoons H_3O^+ + PO_4^{3-} \quad K = 3.98 \times 10^{-13} \end{aligned} \tag{17}$$

where K stands for the corresponding dissociation constants.

Notice in Fig. 8.2 that the equilibrium between the swollen ionic polymer network and its surroundings resembles the situation depicted in Fig. 8.1a where a membrane prevents the solute sugar molecules from entering the pure solvent region. In this case, the polymer acts as a membrane, preventing the charged ions from freely diffusing into the outer solution, establishing a higher concentration of mobile ions inside the network than in the outside (mainly because of the attraction of the fixed ions). There thus exists an associated osmotic pressure arising from the difference in mobile ion concentration. Consequently, in addition to the swelling caused by the entropic mixing of polymer and water solvent, the fixed charges and counterions produce an additional driving force for the network to swell.

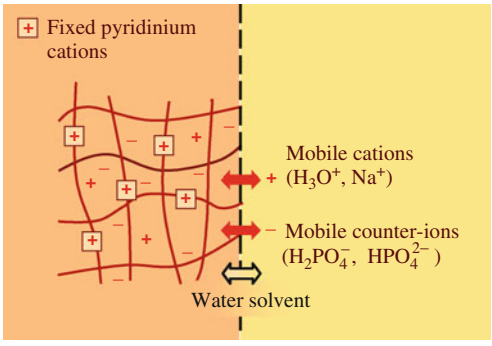

Fig. 8.2 Schematic description of an exchange of ions and solvent between a P4VP polymer network and its surrounding electrolyte. Adapted from Flory [32], Copyright @ 1953 Cornell University and Copyright @ 1981 Paul J. Flory; used by permission of the publisher, Cornell University Press

8.3 Fabrication Procedure

8.3.1 Preparation of the P4VP Responsive Material

In a typical procedure, a solution of P4VP (molecular weight ca. 160,000) in n-butanol (10 mg/ml) is prepared with the reagents used as received. Silicon wafers with a native oxide layer are cut into square pieces ~ 1 cm × 1 cm, and subsequently cleaned either by sonication in isopropyl alcohol for 15 min, or, alternatively, by immersion into piranha solution for 60 min at 80°C followed by thorough cleaning in hot water. (Caution: the piranha solution reacts violently with many organic solvents.) Subsequently, the P4VP solution is spin-coated onto the wafers at 2,000 rpm for 60 s. For crosslinking purposes, the sample is irradiated with a 450-W medium-pressure Mercury lamp (measured intensity of 5 mW/cm^2) for about 5 min. The irradiated films are then soaked in n-butanol for 24 h to remove the unbound polymer. One way to estimate the thickness of the resulting film is to use an ellipsometer. In that case, a value of 1.54 for the refractive index of the P4VP is used in the calculation [39]. This overall procedure gives film thickness in the 60–100 nm range.

8.3.2 Preparation of the Acidic Fountain Tip

A source of hydronium ions H_3O^+ (or, if desired, hydroxide ions OH^- as well) is prepared out of phosphate buffered solutions, which have the remarkable property that can be diluted and still keep the same concentration of H_3O^+. Different pH values can be obtained by dissolving corresponding quantity ratios of sodium dihydrogen phosphate (NaH_2PO_4) and sodium hydrogen phosphate (Na_2HPO_4) in distilled water. For example, mixing 13.8 g/l and 0.036 g/l of the two salts, respectively, gives 0.1 M buffer solution of pH equal to 4.0[2]. This acidic solution serves as the source of hydronium ions which, upon penetrating a P4VP film, protonate the P4VP's pyridyl groups, as suggested in Fig. 8.3 [40]. To achieve the protonation in very localized and targeted regions, however, PEN currently uses a sharp atomic force microscope (AFM) tip as an ion delivery vehicle in a similar fashion to dip-pen nanolithography [2]. For that purpose, as outlined in Fig. 8.4 , an AFM tip of relatively high spring constant ($k = 40$ N/m) is coated by simply soaking the probe into the buffer solution for about 1 min (Fig. 8.4a) and then allowing it to dry in air for 10 min or, alternatively, by blowing it with nitrogen (Fig. 8.4b). Such fountain

[2]Since all phosphate salts are used in hydrated condition, the molecular weight (MW) should include the corresponding portion of water. For NaH_2PO_4 we should include one molecules of water, hence the MW is 137.99. On the other hand, for the Na_2HPO_4 we should consider 7 molecules of water (heptahydrate), which gives a MW of 268.07. Hence, if 13.8 and 0.036 g of NaH_2PO_4 and Na_2HPO_4 are used respectively, then we can quote the concentration of NaH_2PO_4 (the buffer strength) to be practically equal to 0.1 M.

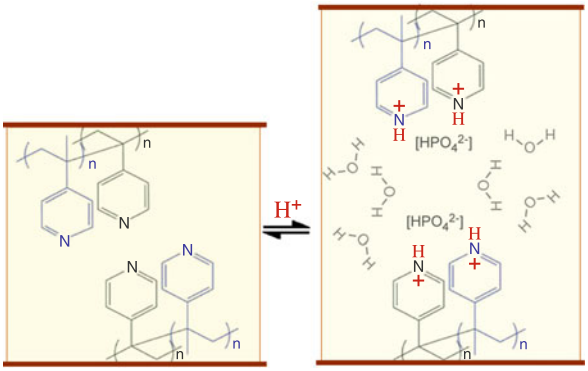

Fig. 8.3 Schematic illustration of the reversible swelling mechanism in P4VP, suggested here to be a consequence of the corresponding electrostatic interaction upon the protonation of the pyridyl groups. Illustration adapted from Maedler et al. [40] and reproduced with permission of the *SPIE*

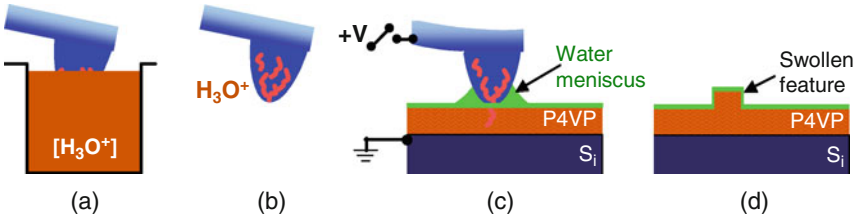

Fig. 8.4 Schematic procedure for attaining spatially-localized protonation of a P4VP film resting on a silicon substrate. After dipping an AFM tip into an acidic buffer solution, the probe is pressed against a P4VP film. The transfer of *hydronium* ions from the tip to the film is aided by the presence of a naturally-formed water meniscus (experiment performed at relative humilities above 40%). The protonation of the P4VP's pyridyl groups triggers the swelling response of the film. The bias voltage helps the process to be more reliable and allows controlling the height of the features

tip constitutes the probe for delivering hydronium ions very locally over targeted sites on a responsive material substrate.

8.3.3 Procedure for the Local Protonation

The fountain-tip is mounted on the head-stage of an AFM system,[3] whose electronic station comprises lithography software for controlling the lateral scanning of the tip along pre-determined paths, and the capability to apply a bias voltage to the probe. The accumulated experimental results suggest that, upon bringing the probe into contact with the polymer film (contact force of $\sim$1 μN), both (i) the surrounding water meniscus that naturally forms between the tip and polymer film,

[3] AFM XE-120 from Park Systems Inc.

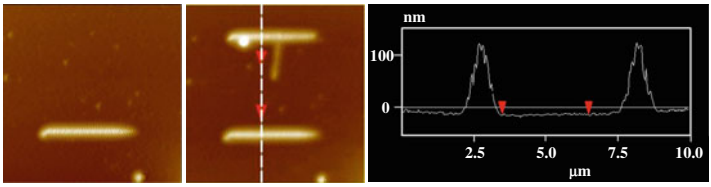

(a)

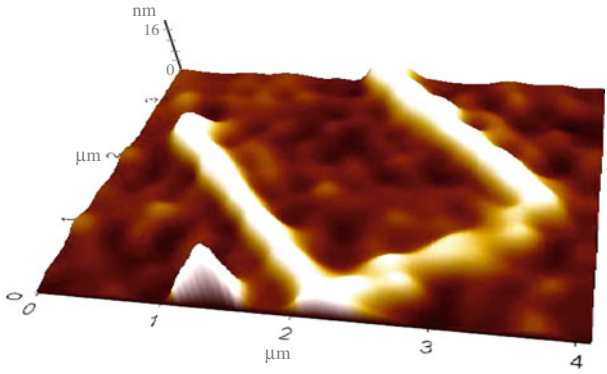

(b)

Fig. 8.5 (**a**) *Top-view images* (10 µm × 10 µm) of two patterns formed sequentially by local protonation of a P4VP film (no electric field was applied). The line profile displays one cross section of the *second image*. (**b**) 3D-view of a "U" shape pattern fabricated on a 4 µm × 4 µm region of another P4VP film (contact force = 1 µN and 5 V tip-sample bias voltage)

and (ii) the buffer concentration gradient, facilitate the transport of hydroium ions from the tip into the polymer (Fig. 8.4c). The subsequent protonation of the P4VP's pyridyl groups (as suggested in Fig. 8.3) gives rise to a net electrostatic repulsion that causes the corresponding polymer region to swell (Fig. 8.4d). However initially successful (see Fig. 8.5a), this simple contact method unfortunately did not guarantee the pattern formation reproducibly. Subsequently we discovered that pattern formation occurred more consistently when applying an electric field between the probe and the substrate.

8.3.4 Pattern Formation

First, with the "ink" loaded tip, an atomic force microscope (AFM) is set in "tapping imaging-mode," where the probe cantilever undergoes oscillations perpendicular to the sample's surface. To obtain an initial knowledge of the "blank paper" (a UV cross-linked P4VP polymer film), an image is taken at a relatively fast lateral scanning rate (5 µm/s). The use of high rates prevents transferring the buffer molecules into the substrate. Subsequently, the microscope is switched to "contact imaging-mode" for pattern formation under physical parameters controlled by the operator,

namely contact forces of the order of 1 μN, "writing" speeds up to 400 nm/s, and fixed bias voltages up to 5 V. Features of different planar morphologies can be generated with pre-programmed software designs, which guide the voltage-controlled XY lateral scanning of the tip while an electronic feedback-control keeps the probe-sample contact force constant. In our case, the sample rests on a XY piezo scanner stage that is equipped with strain-gauge sensors for overcoming piezoelectric hysteresis via another internal feedback control.[4] The tip is held by an independent piezoelectric z-stage, thus conveniently decoupling the sample's horizontal XY scanning motion from the probe's vertical z-displacements. Finally, the microscope is switched back to the tapping mode for topography imaging in order to verify whether the patterns have been formed.

Figure 8.5a shows two sequentially acquired images of the first polymer structures created in our labs by exploiting the responsive characteristics of P4VP. The cross-linked P4VP film swelled only in the areas where the phosphate "ink" was delivered, forming two narrow-line terraces. These two images demonstrate the ability for sequentially creating an initial pattern, then imaging the resulting sample topography with the same ink-loaded tip, and subsequently creating additional patterns. The line profile in Fig. 8.5a reveals that both features are approximately 100 nm in height and 500 nm in width. The relatively large dimensions of these features (compared to the finer patterns we have recently created in our laboratories) may be attributed to the relatively large amount of ink initially attached to the tip (prior to the writing process). That is, after dipping the tip into the buffer, no nitrogen was blown out in front of the "pen" to let it dry; the latter became afterwards a standard practice in our laboratory as a way to evaluate the reproducibility of the fabrication method under similar conditions as possible. The line profile also reveals the hydrogel characteristics of the patterns since the 100 nm constitutes a substantial swelling compared to the initial 80 nm thickness of the polymer film. Unfortunately, the reproducibility of these initial experiments was very poor from day to day, or month to month. At the time when the structures in Fig. 8.5a were created, no electric field was used in the experimental setting.

The reproducibility of the fabrication process greatly improves when an electric field is applied between the silicon tip and the silicon substrate (see setting in Fig. 8.4c). Typical bias voltages are up to 5 V, which when applied through a 50 nm film sets a strong electric field $\sim 10^6$ V/cm (still leaving the film apparently undamaged). Provided that the humidity is above 40%, the patterns are consistently fabricated with this PEN method. Figure 8.5b shows an 8 nm height "*U*" shape structure fabricated under the new procedure, by applying a 5 V bias voltage and under 1 μN contact force. The smaller height of the structures (compared to the ones in Fig. 8.5a) could be attributed to the minimal coating ink on the probe (nitrogen gas is blown on the tip right after dipping it into the buffer solution) thus a lower number of hydronium ions diffused through the polymer network. The lateral dimension of the line-features in both cases presented in Fig. 8.5a, b is limited by

[4] ibid.

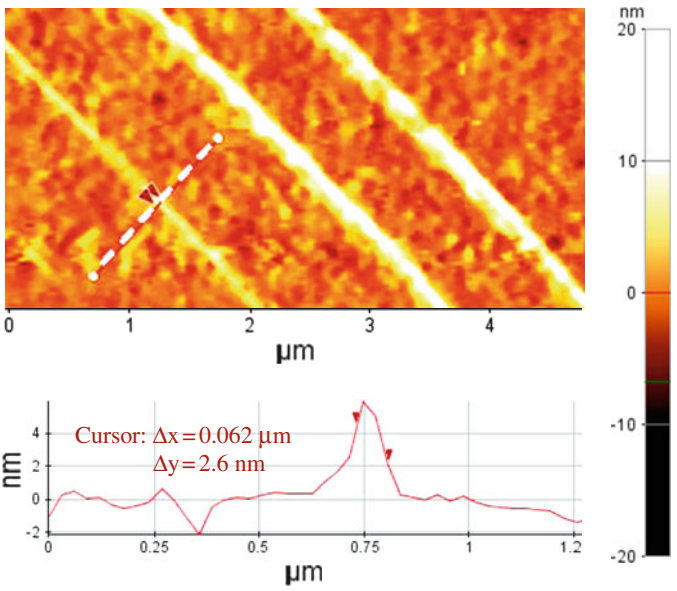

Fig. 8.6 Three line features fabricated at 45% humidity using (form *left* to *right*) contact forces of 0.6, 0.9, 1.0 μN and bias voltages of 5 V, 5 V, and 4 V respectively. The line profile across the line structure at the left displays a line feature ~6 nm tall and ~60 nm wide [41]

the diffusion of hydronium ions into the polymer network. Still, under smaller contact forces and control of the dwelling time, line features as thin as 60 nm can be created, as shown in Fig. 8.6 [41, 42].

The effect of applying an electric field appears straightforward in PEN (Fig. 8.7), helping drive the positive hydronium ions into the polymer network. To provide some context, here we mention other more sophisticated situations where the use of an electric field turns out to be also valuable. For example, an electric field is used to trigger specific conformational transitions switching between straight (hydrophobic) and bent (hydrophobic) states of low-density self-assembled monolayer (SAM) of 16-mercaptohexadecanoic acid on gold, which changes the wettability of the surface while maintaining unaltered the system's environment [43]. Also, nanometer-scale hydrogels, produced by surface grafting of a polymerizable monomer onto Au, undergo reproducible changes in thickness when a potential is applied across the film [44]. More strikingly, an infinitesimal change in electric potential across a polyelectrolyte gel produces volume collapse in polyelectrolyte gels [45]. A broader account on the effects of electric fields on gels has been given by Osada and Gong [33].

The ability of PEN to create patterns having a variety of vertical dimensions in the nanometer range can be capitalized to study molecular interactions in these hydrogel systems with very much detail, including, for example, phase transitions. Polymer gels are known to exist in two phases (swollen and collapsed) where the

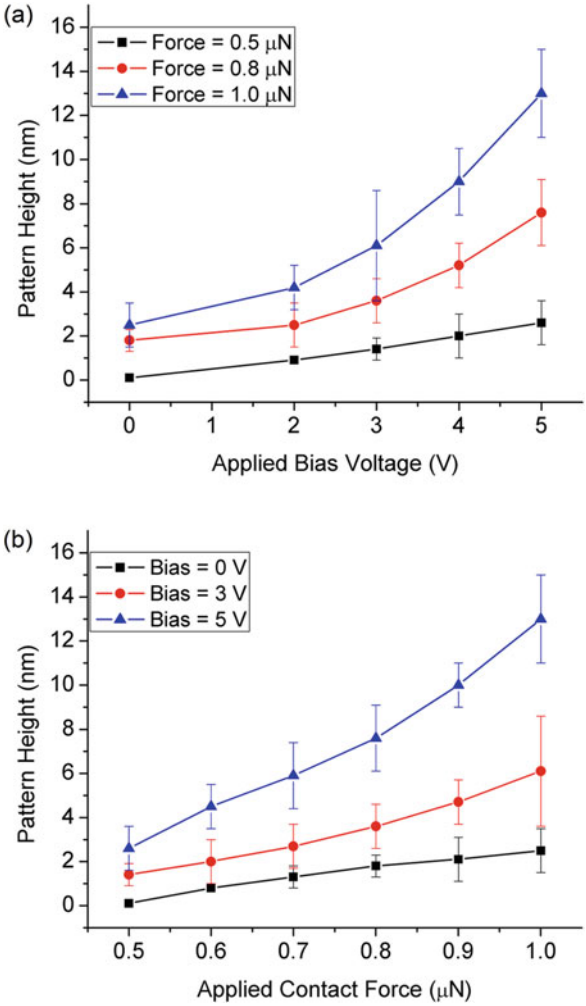

Fig. 8.7 (**a**) Pattern height (nm) vs. applied bias voltage (V) at various fixed contact forces. (**b**) The pattern height (nm) vs. applied contact forces (μN) under different constant bias voltages. Reprinted, with permission, from Wang et al. [42], Copyright @ 2010, American Chemical Society

volume transitions between the phases may occur either continuously or discontinuously [46, 47]. These transitions have been studied by monitoring the swelling as a function of different parameters (solvent quality, temperature [48], pH [49], visible light radiation) [50, 51], which occur as a result of a competition between intermolecular forces (repulsive forces are usually electrostatic whereas attraction is mediated by hydrogen bonding [52], van der Waals interactions, or radiation pressure [53]) that act to expand or shrink the polymer. However, these investigations do not disclose the microscopic view of the structure of gels. While neutron scattering has been used to elucidate these interactions at mesoscopic scales [54], here we have an opportunity to complement these studies with nanoscale-sized individual gels fabricated via PEN.

8.4 Comparison Between PEN and Other DPN Techniques

A characteristic of the PEN technique is the dependence of the pattern dimensions on the positive contact force used to press the tip against the polymer film. The greater the applied external force, the larger the pattern size. This differs greatly from the DPN technique in which the line-width of the pattern is independent of the contact force [55]. DPN works even under gentle negative external forces (where the probe pulls away from the film, but the adhesion forces keep the probe attached to the sample) simply because its underlying mechanism implies just the deposition of molecules on the surface. In PEN, however, the buffer molecules (initially coating the AFM-tip) have to, in addition, penetrate into the polymer substrate. Experimental results indicate that the latter occurs less efficiently with weaker contact forces [56]; see also Fig. 8.7. In fact, no apparent features are formed for contact forces smaller than 0.5 μN (at a writing speed of 80 nm/s), even when applying bias voltages of up to 5 V [42]. Certainly, the longer the dwelling time per pixel (i.e. slower writing speeds), the more hydronium ions diffuse into the polymer thus giving rise to larger patterns [56] which would also allow reducing the contact force. However, extremely long dwell times would make the technique less attractive, thus, a trade off exists between the writing speed and contact force for applying PEN efficiently. (Implementation of PEN in a parallel modality, in order to increase the throughput efficiency, is suggested in Section 8.5 below.)

Confirmation of a contrast difference between DPN and PEN is revealed from test experiments aimed at providing further evidence that the pattern formation in PEN results from the mechanical response of the polymer film and not just the deposition of buffer molecules:

First, when scanning a non-coated tip on a P4VP film under 3 μN contact force, no elevated features were obtained, as shown in Fig. 8.8a [56]. Only scratches of 2 nm deep resulted from this operation, as evidenced by the line profile; the cross section indicates that the observed small protuberances are the result removed material from the scratches. This result suggests that a buffer solution is needed for the creation of PEN patterns.

Second, an argument could be made about whether or not, when using a coated tip, the patterns could result from the physical deposition of buffer molecules. To refute this argument, this time the test experiment was carried out using a buffer-coated tip scanned at low speed over a non-responsive polymer, polystyrene. The result presented in Fig. 8.8b shows no pattern formation, thus providing favorable evidence that features created were not just the deposition of buffer molecules on a polymer surface, but the swelling response of the substrate itself when using responsive materials.

Third, the results given above also favor the hypothesis of protonation. But would the hydronium ions be the only ones diffusing into the polymer network? To test this hypothesis C. Maedler et al. investigated the swollen structures [57]. Armed with Kelvin Probe Force Microscopy as a tool [58], and following up studies of deposition of charges in silicon [57], they

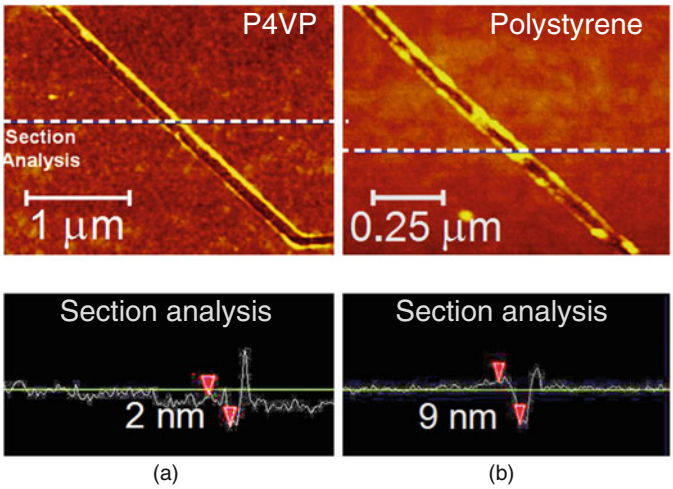

Fig. 8.8 (**a**) Scanning along a diagonal path with a contact force of 3 μN on a P4VP film, using an uncoated tip, produces only scratches, as revealed by the cross section line profile. (**b**) Image of the resulting topography produced by a line scan on a polystyrene film (a non responsive material) using a contact force of 2 μN and a coated tip. A cross section line profile reveals only a scratch indent in the substrate. Reprinted, with permission, from Maedler et al. [56], copyright 2008, American Institute of Physics

corroborated to have the sensitivity for monitoring the presence of a net charge in the polymer structures, if any. They found none. This implies that not only the hydronium ions penetrate the polymer, but they bring with them their corresponding counterions (see expression (17) above), thus keeping the charge neutrality of the sample.

DPN and PEN agree on the role played by the humidity. PEN pattern formation in P4VP films under different humidity levels has been well documented by C. Maedler [40, 56] and X. Wang [42]. No features formation occurs below 40% of relative humidity, suggesting that a water meniscus [59] naturally created between the probe and the polymer film plays a key role. In this regard, there is a coincidence of arguments with the DPN community that supports the hypothesis that a water meniscus is a fundamental component for the technique to work [60]. There is evidence that a liquid bridge exists even at zero humidity conditions [61]. (However, some authors have concluded that a meniscus is not involved in DPN experiments with certain molecules like 1-octadecanethiol [62]).

Finally, the reversibility of PEN contrasts with the, in general, non-reversible character of DPN. An exception to this notion is observed, however, in one DPN application where a voltage biased tip is used to create positive and negative charged nanopatterns on 1-hexadecanethiol (HDT) self-assembled monolayers (SAMs) on Au. The positive nanopatterns are gold oxide, which can be reduced back to gold by ethanol ink via DPN [63]. This development followed the "molecular eraser" [64]

where a tip with a negative bias voltage (relative to the electrically grounded substrate that contain a monolayer of MHA 16-mercaptohexadecanoic acid) causes the molecules to desorb. Thus, regions of the alkanethiol can be selectively removed, which constitutes the pattern. The recessed areas can be refilled via DPN thus erasing the pattern. On the other hand, PEN instead is an intrinsically reversible process, using a base ink to erase the pillars previously formed by the acidic ink. The reversibility of the process was elegantly implemented by X. Wang et al. [42] using the same tip but inked with a basic phosphate buffer solution of pH 8.3, this time without applying a bias voltage. The removal of a pre-fabricated pillar structure was performed by keeping the tip in contact and stationary on top of the pillar. Results showed the progressive attenuation of the height of the structure. The basic buffer neutralizes the pyridinium converting it to the neutral pyridyl group and causing the film to "de-swell".

On the other hand, PEN differs from Electrochemical AFM Dip-Pen Nanolithography [65, 66], where the tiny condensed water between the tip and the substrate is used as a nanometer-sized electrochemical cell in which metal salts (coating the probe) are dissolved, reduced into metals electrochemically, and deposited onto the surface. This method was used first to deposit Pt on a silicon substrate. The process involves coating an AFM cantilever tip with H_2PtCl_6 and applying a positive voltage to the tip relative to the electrically grounded substrate (the latter constituted by silicon with its native oxide). Despite the oxide, the conductivity is sufficient for the reduction (electrons gain) of the precursor ions $PtCl_6^{2-}$. During the process, H_2PtCl_6 dissolved in the water meniscus is electrochemically reduced from Pt(IV) to Pt(0) metal at the (cathode) silicon surface and deposits as Pt according to the reduction reaction $PtCl_6^{2-} + 4e \rightarrow Pt + 6Cl^-$. (The DC voltages are kept in the 1–4 V; higher voltages would tend to oxidize the silicon substrate and form SiO_2 instead of Pt nanostructures.) Electrochemical AFM Dip-Pen Nanolithography is therefore a technique were the deposited materials constitute the nanostructure, similar to DPN but different than PEN.

PEN is also different from Constructive Nanolithography (CNL) [67, 68] and its similar Electro Pen Nanolithography (EPN) [69]. Contrasting Electrochemical AFM Dip-Pen Nanolithography (described above), whose working principle is based on *reducing* (gaining of electron) a precursor ion, CNL and EPN exploit an *oxidation* (loss of electron) process instead. In one application of CNL, a silicon substrate is first coated with a 2.5 nm thick monolayer of octadecyltrichlorosilane (OTS, an organic molecule with a methyl-terminated,18-carbon alkyl chain), which serves as the initial blanket surface to be oxidized on specific regions by the apex of a conductive AFM tip. The oxidation process is implemented by applying a positive bias voltage to the substrate relative to the tip (the latter kept at electrical ground). As a result, the oxidized areas (initially hydrophobic, neutral, and inert) become hydrophilic, negative-charged, and chemically active, forming the multifunctional templates for post, or in-situ, surface generation of organic (insulator), metal, or semiconductor nanocomponent features, including the implementation of a wetting-driven patterning [70, 71]. The post pattern generation process of CNL is elegantly alleviated in EPN where the electrically biased conductive AFM tip is

also coated with ink (trialkoxysilane and quaternary ammonium salts), which are in situ transferred during the scanning process as the local oxidation occurs. The virtue of CNL and EPN is that the transfer of molecules occurs only on the regions that have been oxidized, which can be as small as 25 nm, thus bypassing the diffusion effect that limit the lateral resolution of DPN. CNL and EPN therefore have characteristics similar to DPN, hence different than PEN, for their patterns are constituted by anchoring molecules on the substrate, although a chemically modified substrate.

PEN is more alike to Chemical Lithography (ChemLith) [72]. This technique exploits the fact that photoresist materials change their solubility upon an acid-catalyzed chemical reaction. As an alternative to the diffraction limited photolithography method (where the photoacid generator is mixed in the resist formula and the acid is generated by photon-initiated reactions), ChemLith delivers the catalyzing acid proton source to the desired position on a negative resist film via either a nanoimprinting method or by using an sharp stylus. In a post bake step, the resist molecules are catalyzed to cross-link with each other, and thus become insoluble in the final development step. Thus ChemLith nanopatterns result from a local protonation process (similar to PEN) and a post baking step (the latter renders the process irreversible, unlike PEN).

As mentioned at the beginning of this chapter, PEN joins other efforts for developing responsive materials (including polymer nano-composites [73], soft hydrogels [3, 7] and chemically functionalized metal nanoparticles [15, 74], which may also be driven by proton sources as well as the use of bias voltages), but putting emphasis into the nanoscale size regime. This PEN development occurs in parallel to other electrochemistry SPM-based efforts for fabricating energy storage devices [75], and, more generally, for attaining reliable surface modification using SPM [76, 77].

8.5 Perspectives

We have introduced Proton-fountain Electric-field-assisted Nanolithography (PEN) as a technique for fabricating erasable nanostructures that closely mimic natural bio-environments. Its distinct feature, contrasting other DPN-based techniques, resides in the fact that the pillar patterns are made of the substrate material itself (a polymer film). The pattern formation results from the delivery of hydronium ions through an acidic-fountain tip in contact with the substrate, causing the polymer film to swell at targeted locations. In addition, the patterns can be erased with a basic-ink loaded tip. Such a reversible character of the fabrication process could be relevant to a wide range of potential applications, ranging from microelectronics (the swollen and no-swollen states could represent the ones and zeros in a memory device) to biotechnologies (variable size gates that open and close compartment in micro- and nano-fluidic devices used for separation of molecules or chemical reagents). Further, its capability for controlling the dimension of the patterns with nanometer precision, via an electric field, offers an opportunity to use these films as

testbed for studying fundamental (thermodynamic and kinetic) physical properties of responsive materials at the nanoscale level. This is concomitant to the far reaching goal towards developing thin film-based responsive materials that can selectively respond to a variety of external stimuli (mechanical, chemical, optical, and changes in environmental conditions).

Despite its current progress, PEN would benefit from further development in order to place the technique in more solid grounds. For example, it would be convenient to study with more detail the effects of humidity (at different levels) in conjunction with the application of a range of bias voltages; until now their effects have been reported only separately. The objective would be to understand, optimize, and to know better, the dynamics involved in the transportation of hydronium-ions from the tip to inside the polymer network. This study would also help to elucidate why relatively strong forces ($\sim\mu$N) are needed for a rapid pattern formation to occur in PEN. Apparently, the first monolayers of water [78, 79], found naturally adsorbed on the polymer film, is the first barrier that the ions from the tip face before rapidly diffusing into the polymer film. Functionalizing the responsive polymer film with, in turn, hydrophobic or hydrophilic layers would help to contrast this hypothesis. In passing, the latter proposed experiment could also lead to the formation of the thinnest line feature under DPN, for by writing on an hydrophobic-functionalized responsive-material film, only the region in contact with the tip would create a richer water content bridge for the hydronium ions to penetrate into the polymer network. Certainly the thinnest line width would be determined by the diffusion of the ions while inside the polymer; still, the degree of cross-link of the starting material polymer film could be used to influence this diffusion, which offers another variable to control the ultimate resolution in PEN.

To gain versatility on the PEN implementation, and with a perspective on application for building memory devices (the reversibility of the PEN allowing the implementation of memory level changes), it would be worth to explore the use of solid state sources of protons [72, 80, 81]. Such an application could benefit from current efforts for developing solid acid materials as electrolytes in fuel cells [82, 83]. In that direction of technological applications, it would be worth to also explore the implementation of PEN in a parallel format; that is, to develop capability for fabricating many patterns at once. For this application, PEN can capitalize on the fact that relatively strong forces are needed to fabricate the patterns, which provides some leverage to implement a stamping type fabrication modality. For example, metallic (master) features can be fabricated on a flat (glass) substrate, all of them interconnected as to be able to apply a bias voltage. After spin-coating a layer of buffer solution on the metallic master features, the resulting wet stamp would be pressed against a P4VP film. By applying a bias voltage, the protonation would be more effective on the regions defined by the metallic features, hence the patterns from the master stamp will be replicated onto the polymer substrate by its swelling reaction. Further, this methodology could become very versatile, since different metallic regions on the master stamp could be electrically addressed at will; thus a given mask would be used for fabricating different patterns according to a programmable voltage pattern.

Finally, it is worth to point out that the intrinsic hydrogel nature of the P4VP patterns fabricated with PEN constitutes an advantage in applications that involve the replication of structures that closely mimic natural bio-environments. This capability is particularly relevant to a recent trend in research that conceives the cell not only as a chemical factory but also as a sensitive mechanical device. Incidentally, it has recently been reported that stem cells do not regenerate efficiently in vitro environment unless the surrounding medium is made out of flexible gels [84]. Hence, further developments on PEN should benefit the implementation of these attractive bio-engineering applications.

References

1. K. Salaita, Y. Wang, and C. A. Mirkin, "Applications of dip-pen nanolithography," *Nat. Nanotechnol.* **2**, 145 (2007).
2. R. D. Piner, J. Zhu, F. Xu, S. Hong, and C. A. Mirkin, "Dip-Pen nanolithography," *Science* **283**, 661 (1999).
3. I. Tokarev and S. Minko, "Stimuli-responsive hydrogel thin films," *Soft Matter* **5**, 511 (2009).
4. L. Anson, "Membrane protein biophysics," *Nature* **459**, 343 (2009).
5. C. Ainsworth, "Stretching the imagination," *Nature* **456**, 696 (2008).
6. B. Bhushan, "Biomimetics: lessons from nature-an overview," *Phil. Trans. R. Soc. A* **367**, 1445 (2009).
7. I. Tokarev, M. Motornov, and S. Minko;, "Molecular-engineered stimuli-responsive thin polymer film: a platform for the development of integrated multifunctional intelligent materials," *J. Mater. Chem*. **19**, 6932 (2009).
8. C. Cofield, "Cell is mechanical device," *Am. Phys. Soc., APS News*, Series II, **19**, 4 (June 2010).
9. C. Wu, Y. Li, J. H. Haga, R. Kaunas, J. Chiu, F. Su, S. Usami, and S. Chien, "Directional shear flow and Rho activation prevent the endothelial cell apoptosis induced by micro patterned anisotropic geometry," *PNAS* **104,** 1254 (2007).
10. C. S. Chen, M. Mrksich, S. Huang, G. M. Whitesides, and D. E. Ingber, "Geometric control of cell life and death," *Science* **276**, 1425 (1997).
11. M. A. Greenfield, J. R. Hoffman, M. Olvera de la Cruz, and S. I. Stupp, "Tunable mechanics of peptide nanofiber gels," *Langmuir* **26**, 3641 (2010).
12. M. M. Stevens and J. H. George, "Exploring and engineering the cell surface interface," Science **310**, 1135 (2005).
13. S. Maeda, Y. Hara, T. Sakai, R. Yoshida, and S. Hashimoto, "Self-walking gel,**"** *Adv. Mater.* **19**, 3480 (2007).
14. T. K. Tam, M. Ornatska, M. Pita, S. Minko, and E. Katz, "Polymer brush-modified electrode with switchable and tunable redox activity for bioelectronic applications," *J. Phys. Chem. C* **112**, 8438 (2008).
15. D. Wang, I. Lagzi, P. J. Wesson, and B. A. Grzybowski, "Rewritable and pH-sensitive micropatterns based on nanoparticle 'Inks'," *Small* **6**, 2114 (2010).
16. J. Ruhe, M. Ballauff, M. Biesalski, P. Dziezok, F. Grohn, D. Johannsmann, N. Houbenov, N. Hugenberg, R. Konradi, S. Minko, M. Motornov, R. R. Netz, M. Schmidt, C. Seidel, M. Stamm, T. Stephan, D. Usov, and H. Zhang, "Polyelectrolyte brushes" in: "Polyelectrolytes with Defined Molecular Architecture," M. Schmidt Ed. *Adv. Polym. Sci*. **165**, 79 (2004).
17. C. Liu, H. Qin, and P. T. Mather, "Review of progress in shape-memory polymers," *J. Mater. Chem.* **17**, 1543 (2007).
18. R. Yoshida, K. Uchida, Y. Kaneko, K. Sakai, A. Kikuchi, Y. Sakurai, and T. Okano, "Comb-type grafted hydrogels with rapid deswelling response to temperature changes," *Nature* **374**, 240 (1995).

19. T. Suzuki, S. Shinkai, and K. Sada, "Supramolecular crosslinked linear poly(trimethylene iminium trifluorosulfonimide) polymer gels sensitive to light and thermal stimuli," *Adv. Mater.* **18**, 1043 (2006).
20. B. A. Evans, A. R. Shields, R. Lloyd Carroll, S. Washburn, M. R. Falvo, and R. Superfine, "Magnetically actuated nanorod arrays as biomimetic cilia," *Nano Lett.* **7**, 1428 (2007).
21. O. Ikkala and G. Brinke, "Functional materials based on self assembly of polymeric supramolecules," *Science* **295**, 2407 (2002).
22. M. Kaholek, W. K. Lee, B. LaMattina, K. C. Caster, and S. Zauscher, "Fabrication of stimulus-responsive nanopatterned polymer brushes by scanning-probe lithography," *Nano Lett*. **4**, 373 (2004).
23. X. Liu, S. Guo, and C. A. Mirkin, "Surface and site-specific ring-opening metathesis polymerization initiated by dip-pen nanolithography," *Angew. Chem. Int. Ed*. **42**, 4785 (2003).
24. Y. Okawa and M. Aono, "Nanoscale control of chain polymerization," *Nature* **409**, 683 (2001).
25. S. P. Sullivan, A. Schnieders, S. K. Mbugua, and T. P. Beebe Jr., "Controlled polymerization of substituted diacetylene self-organized monolayers confined in molecule corrals," *Langmuir* **21**, 1322 (2005).
26. Y. Okawa, D. Takajo, S. Tsukamoto, T. Hasegawa, and M. Aono, "Atomic force microscopy and theoretical investigation of the lifted-up conformation of polydiacetylene on a graphite substrate," *Soft Matter* **4**, 1041 (2008).
27. P. Calvert, "Hydrogels for soft machines," *Adv. Mater*. **21**, 743 (2009).
28. P. J. Flory and J. Rehner, "Statistical mechanics of cross-linked polymer networks I. Rubberlike elasticity," *J. Chem. Phys*. **11**, 512 (1943).
29. P. J. Flory and J. Rehner, "Statistical mechanics of cross-linked polymer networks II. Swelling," *J. Chem. Phys*. **11**, 521 (1943).
30. K. Huang, "Statistical Mechanics," Wiley, New York, 2nd Ed. (1987).
31. F. P. Chinard and T. Enns, "Osmotic pressure," *Science* **124**, 472 (1956).
32. P. J. Flory, "Principles of Polymer Chemistry," Cornell University Press, Oxford (1969).
33. Y. Osada and J. Gong, "Soft and wet materials: Polymer gels," *Adv. Mater*. **10**, 827 (1998).
34. L. D. Landau and E. M. Lifshitz, "Statistical Physics", Elsevier, New York, 3rd Ed., Part 1, pp. 72, 267 (2006).
35. P. J. Flory, "Thermodynamics of high polymer solutions," *J. Chem. Phys*. **10**, 51 (1942).
36. P. J. Flory, "Statistical mechanics of swelling of network structures," *J. Chem. Phys*. **18**, 108 (1950).
37. W. Hu and D. Frenkel, "Lattice-model study of the thermodynamic interplay of polymer crystallization and liquid–liquid demixing," *J. Chem. Phys.* **118**, 10343 (2003).
38. A. Yu. Grosberg and A. R. Khokhlov, "Giant Molecules. Here, There and Everywhere," Academic Press, New York (1997).
39. D. Woo, "Spectroscopic Ellipsometry Studies of Polymers on Silicon Wafer," Thesis for the Master degree in Physics, Portland State University, Portland, OR (2009).
40. C. Maedler, H. Graaf, S. Chada, M. Yan, and A. La Rosa, "Nano-structure formation driven by local protonation of polymer thin films", *Proc. SPIE*, **7364**, 736409-1 (2009).
41. X. Wang, "Characterization of Mesoscopic Fluid-Like Films with the Novel Shear-Force/Acoustic Microscopy," Thesis for the Master degree in Physics, Portland State University, Portland, OR (2010).
42. X. Wang, X. Wang, R. Fernandez, L. Ocola, M. Yan, and A. La Rosa, "Electric field-assisted dip-pen nanolithography on poly(4-vinyl pyridine) films," *ACS Appl. Mater. Interface* **2**, 2904–2909 (2010).
43. J. Lahann, S. Mitragotri, T. Tran, H. Kaido, J. Sundaram, I. S. Choi, S. Hoffer, G. A. Somorjai, and R. Langer, "A reversibly switching surface," *Science* **299**, 371 (2003).
44. I. S. Lokuge and P. W. Bohn, "Voltage-tunable volume transitions in nanoscale films of poly(hydroxyethyl methacrylate) surfaces grafted onto gold," *Langmuir* **21**, 1979 (2005).

45. T. Tanaka, I. Nishio, S. Sun, and S. Ueno-Nishio, "Collapse of gels in an electric field," *Science*, **218**, 467 (1982).
46. M. Annakaand and T. Tanaka, "Multiple phases of polymer gels," *Nature* **355**, 430 (1992).
47. A. Matsuyama, "Volume phase transitions of smectic gels," *Phys. Rev. E* **79**, 051704 (2009).
48. W. Xue, and I. W. Hamley, "Thermoreversible swelling behaviour of hydrogels based on *N*-isopropylacrylamide with a hydrophobic comonomer," *Polymer* **43**, 3069 (2002).
49. A. Richter, G. Paschew, S. Klatt, J. Lienig, K. Arndt, and H. P. Adler, "Review on hydrogel-based pH sensors and microsensors," *Sensors* **8**, 561 (2008).
50. T. Tanaka, D. Fillmore, S.-T. Sun, I. Nishio, G. Swislow, and A. Shah, "Phase transitions in ionic gels," *Phys. Rev. Lett.* **45**, 1636 (1980).
51. A. Suzuki and T. Tanaka, "Phase transition in polymer gels induced by visible light," *Nature* **346**, 345 (1990).
52. F. Ilmain, T. Tanaka, and E. Kokufuta, "Volume transition in a gel driven by hydrogen bonding," *Nature* **349**, 400 (1991).
53. S. Juodkazis, N. Mukai, R. Wakaki, A. Yamaguchi, S. Matsuo, and H. Misawa, "Reversible phase transitions in polymer gels induced by radiation forces," *Nature* **408**, 178 (2000).
54. M. Shibayama and T. Tanaka, "Small-angle neutron scattering study on weakly charged temperature sensitive polymer gels," *J. Chem. Phys*. **97**, 6842 (1992).
55. S. Hong and C. A. Mirkin, "A nanoplotter with both parallel and serial writing capabilities," *Science* **288**, 1808 (2000).
56. C. Maedler, S. Chada, X. Cui, M. Taylor, M. Yan, and A. La Rosa, "Creation of nanopatterns by local protonation of P4VP via dip pen nanolithography." *J. Appl. Phys*. **104**, 014311 (2008).
57. C. Maedler, "Applying Different Modes of Atomic Force Microscopy for the Manipulation and Characterization of Spatially Localized Structures and Charges," Diploma Thesis for the academic degree of Diplom Physiker; Faculty of Natural Sciences Institute of Physics, Chemnitz University of Technology (2009).
58. M. Nonnenmacher, M. P. O'Boyle, and H. K. Wickramasinghe, "Kelvin probe force microscopy," *Appl. Phys. Lett.* **58**, 2921 (1991).
59. M. Schenk, M. Futing, and R. Reichelt, "Direct visualization of the dynamic behavior of water meniscus by scanning electron microscopy," *J. Appl. Phys.* **84**, 4880 (1998).
60. L. M. Demers, D. S. Ginger, Z. Li, S.-J. Park, S.-W. Chung, and C. A. Mirkin, "Direct patterning of modified oligonucleotides on metals and insulators by dip-pen nanolithography," *Science* **296**,1836 (2002).
61. S. Rozhok, P. Sun, R. Piner, M. Lieberman, and C. A. Mirkin, "AFM study of water meniscus formation between an aFM tip and NaCl substrate," *J. Phys. Chem. B* **108**, 7814 (2004).
62. P. E. Sheehan and L. J. Whitman, "Thiol diffusion and the role of humidity in 'dip pen nanolithography'," *Phys. Rev. Lett*. **88**, 156104 (2002).
63. Z. Zheng, M. Yang, and B. Zhang, "Reversible nanopatterning on self-assembled monolayers on gold," *J. Phys. Chem. C* **112**, 6597 (2008).
64. J.-W. Jang, D. Maspoch, T. Fujigaya, and C. A. Mirkin, "A 'molecular eraser' for dip-pen nanolithography," *Small* **3**, 600 (2007).
65. Y. Li, B. W. Maynor, and J. Liu, "Electrochemical AFM 'Dip-pen' nanolithography," *J. Am. Chem. Soc*. **123**, 2105 (2001).
66. F. C. Simeone, C. Albonetti, and M. Cavallini, "Progress in micro- and nanopatterning via electrochemical lithography," *J. Phys. Chem. C* **113**, 18987 (2009).
67. R. Maoz, E. Frydman, S. R. Cohen, and J. Sagiv, "'Constructive nanolithography': inert monolayers as patternable templates for in-situ nanofabrication of metal-semiconductor-organic surface structures: a generic approach," *Adv. Mater.* **12**, 725 (2000).
68. Z. Zheng, M. Yang, and B. Zhang, "Constructive nanolithography by chemically modified tips: nanoelectrochemical patterning on SAMs/Au," *J. Phys. Chem. C* **114**, 19220 (2010).
69. Y. Cai and B. M. Ocko, "Electro pen nanolithography," *J. Am. Chem. Soc*. **127**, 16287 (2005).
70. D. Chowdhury, R. Maoz, and J. Sagiv, "Wetting driven self-assembly as a new approach to template-guided fabrication of metal nanopatterns," *Nano Lett.* **7**, 1770 (2007).

71. A. Zeira, D. Chowdhury, S. Hoeppener, S. T. Liu, J. Berson, S. R. Cohen, R. Maoz, and J. Sagiv, "Patterned organosilane monolayers as lyophobic−lyophilic guiding templates in surface self-assembly: monolayer self-assembly versus wetting-driven self-assembly," *J. Langmuir* **25**, 13984 (2009).
72. P. Yao, G. J. Schneider, J. Murakowski, and D. W. Prather, "Chemical lithography," *J. Vac. Sci. Technol. B* **24**, 2553 (2006).
73. K. Shanmuganathan, J. R. Capadona, S. J. Rowan, and C. Weder, "Stimuli-responsive mechanically adaptive polymer nanocomposites," *ACS Appl. Mater. Interface* **2**, 165 (2010).
74. R. Klajn, P. J. Wesson, K. J. M. Bishop, and B. A. Grzybowski, "Writing self-erasing images using metastable nanoparticle 'Inks'," *Angew. Chem. Int. Ed*. **48**, 7035 (2009).
75. S. V. Kalinin and N. Balk, "Local Electrochemical functionality in energy storage materials and devices by scanning probe microscopies: status and perspectives," *Adv. Mater.* **22**, E193–E209 (2010).
76. A. A. Tseng, A. Notargiacomo, and T. P. Chen, "Nanofabrication by scanning probe microscope lithography: a review," *J. Vac. Sci. Technol. B* **23**, 877 (2005).
77. A. A. Tseng, A. Notargiacomo, T. P. Chen, and Y. Liu, "Profile uniformity of overlapped oxide dots induced by atomic force microscopy," *J. Nanosci. Nanotechnol.* **10**, 4390 (2010).
78. K. B. Jinesh and J. W. M. Frenken, "Capillary condensation in atomic scale friction: how water acts like a glue," *PRL* **96**, 166103 (2006).
79. P. J. Feibelman, "The first wetting layer on a solid," *Physics Today* **63**, 34 (2010).
80. E. Kapetanakis, A. M. Douvas, D. Velessiotis, E. Makarona, P. Argitis, N. Glezos, and P. Normand, "Hybrid organic–inorganic materials for molecular proton memory devices," *Org. Electron.* **10**, 711 (2009).
81. E. Kapetanakis, A. M. Douvas, D. Velessiotis, E. Makarona, P. Argitis, N. Glezos, and P. Normand, "Molecular storage elements for proton memory devices," *Adv. Mater*. **20**, 4568 (2008).
82. S. M. Haile, D. A. Boysen, C. R. Chisholm, and R. B. Merle, "Solid acids as fuel cell electrolytes," *Nature* **410**, 910 (2001).
83. T. Norby, "The promise of protonics," *Nature* **410**, 877 (2001).
84. P. M. Gilbert, K. L. Havenstrite, K. E. G. Magnusson, A. Sacco, N. A. Leonardi, P. Kraft, N. K. Nguyen, S. Thrun, M. P. Lutolf, and H. M. Blau, "Substrate elasticity regulates skeletal muscle stem cell self-renewal in culture," *Science* **329**, 1078 (2010).